J Therm Anal Calorim (2010) 102:923–930
DOI 10.1007/s10973-010-0804-y

Analysis of decomposition processes of ausferrite in copper–nickel austempered ductile iron

Andrzej Gazda

Received: 29 January 2010 / Accepted: 13 April 2010 / Published online: 6 May 2010

Abstract Analysis of thermal decomposition processes of the ausferrite obtained during simulation of austempering heat treatment was performed on austempered ductile iron (ADI). The analysis method consisting in investigation of inverse phase transformations was applied. The material with specified phase composition and well-defined thermophysical properties, both resulting from the conducted heat treatment cycle, was heated under controlled conditions and the thermal effects—enthalpy change and volume change were recorded by means of differential scanning calorimetry (DSC) and differential dilatometry. The process of ausferrite decomposition in the range of 100–800 °C was discussed; the identification scheme and temperature sequence of phase transformations accompanying the ausferrite decomposition were established. The elaborated decomposition scheme allows selection of the ADI heat treatment and its optimization by means of the non-isothermal thermal analysis methods.

Keywords Austempered ductile iron · ADI · DSC · Dilatometry · Ausferrite decomposition

Introduction

The structure and mechanical properties of austempered ductile iron (ADI) depend strongly on the mechanism and kinetics of phase transformations proceeding successively during the austempering heat treatment consisting in quenching followed by isothermal transformation:

1. $\gamma(C_o) \rightarrow \alpha_{ac} + \gamma_s\,(C)$ (1)
2. processing window: stability of structure $\alpha_{ac} + \gamma_s$ (C)
3. $\gamma_s(C) \rightarrow \alpha + Fe_3C$ (or ε carbide) (2)

During the first stage of isothermal austenite $\gamma(C_o)$ decomposition, ausferrite with fine acicular ferrite α_{ac} and meta-stable reacted carbon-saturated austenite γ_s (C) is created (1).

As a result of the optimum heat treatment (processing window), ausferrite with maximum amount of fine acicular ferrite α_{ac} and reacted stable carbon-saturated austenite γ_s (C) is formed. Proper choice of austempering heat treatment parameters (dwell time at constant temperature) prevents martensite or carbides formation and results in mechanical properties which satisfy requirements defined by ASTM A 897 standard.

The prolonged time of isothermal transformation (third step) results in decomposition of carbon-rich austenite with precipitation of cementite and/or carbide ε according to the formula (2).

ADI is characterized by good machinability, high strength-to-weight ratio, good wear resistance and damping capacity, and outstanding mechanical properties—toughness and fatigue strength.

Designing of ADI castings with defined mechanical properties requires the establishing a correlation between structure sensitive parameters and mechanical properties to be applied in heat treatment simulation.

In this process, very useful is the analysis of inverse phase transformations, i.e., of the decomposition of metastable phases produced during ADI heat treatment, carried out by means of non-isothermal thermal analysis methods.

First order phase transformations are characterized by non-zero entropy (or enthalpy) ($\Delta H \neq 0$) and volume

A. Gazda (✉)
Center of High Temperature Studies, Foundry Research Institute, 73 Zakopianska St., 30-418 Krakow, Poland
e-mail: agazda@iod.krakow.pl

changes ($\Delta V \neq 0$), so both calorimetric (DSC) and dilatometric methods are very suitable and useful here.

These methods, complementary to microscopic observations, depend upon controlled heating of well structure-defined material and recording changes in thermophysical properties (enthalpy and volume) initiated by decomposition of the initial phases. Calorimetric and dilatometric methods are used successfully to study precipitation and dissolution reactions in various heat treatable alloys [1–3].

The ausferrite stability depends on isothermal transformation conditions and is sensitive to the heating rate of non-isothermal decomposition processes, such as diffusional processes of carbon precipitation and dissolution. It implies the necessity of the uniformity of measurement conditions to obtain comparable results.

The aim of this paper is the complex analysis of calorimetric and dilatometric curves resulting from the decomposition of ausferrite structure. There are many literature sources devoted to the problem of iron-based martensite tempering [1, 4–7], but there is no complex analysis of ausferrite decomposition in a wide range of temperatures. The analysis will allow identification of the scheme and temperature sequence of the proceeding phase transformations and this will supply useful means to establish and test optimum heat treatment parameters.

Preparation of materials

Chemical composition of the investigated base ductile iron was (in wt%): C = 3.70; Si = 2.50; Cu = 0.90, and Ni = 1.37. The B2 symbol of alloy designation was preserved because this alloy was chosen from a group of ductile irons under more detailed investigations [8]. The typical as-cast ductile iron microstructure is shown in Fig. 1a and b.

As a result of austempering characterized by the following heat treatment parameters: temperature and time of austenitizing, temperature (T_{pi}) and holding time (t_{pi}) of isothermal transformation, a set of ADI samples with various morphologies was obtained.

The following schedule of austempering heat treatment was designed:

- austenitizing at $T_a = 900$ °C for $t_a = 60$ min;
- quenching followed by isothermal transformation at 270, 350, and 390 °C for several holding times to obtain various stages of ausferrite growth.

Dwell times given in bold characters (column 5 in Table 1) indicate the values for processing window of the examined alloy, i.e., the optimum austempering heat treatment parameters: 120 min at 270 °C, 60 min at 350 °C, and 45 min at 390 °C.

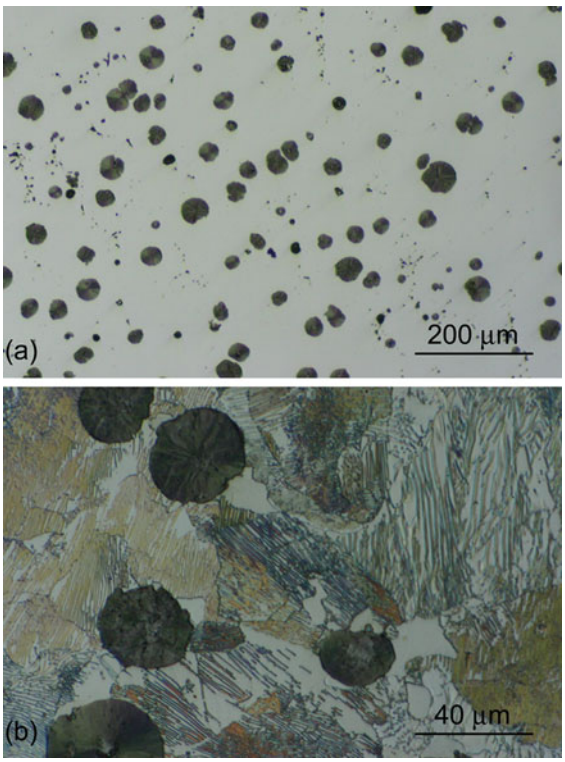

Fig. 1 Microstucture of alloy B2; (**a**) metallographic cross-section after polishing, (**b**) metallographic cross-section after etching

Table 1 Parameters of ADI heat treatment

T_{pi}/°C	Time of isothermal transformation t_{pi}/min					
	1	2	3	4	5	6
270	20	40	60	80	**120**	160
350	5	15	30	45	**60**	90
390	5	10	20	30	**45**	60

Experimental

Using dynamic dilatometric and DSC methods, the qualitative analysis of phase transitions accompanying the decomposition of ADI with differentiated structure resulting from different heat treatment parameters was performed.

ADI samples were heated at a rate of 5 K/min in argon protective atmosphere in a Linseis L76 dilatometer and thermal expansion $\Delta L/L$ curves were recorded. The dilatometric curves in the form of thermal expansion coefficient $\beta(T)$, obtained by numerical differentiation of $\Delta L/L$ curves, make the identification of phase transformations much easier.

To assure comparable measurement conditions, ADI samples were heated at a rate of 5 K/min in argon protective atmosphere in a Netzsch DSC 404C, and DSC

curves were recorded. To establish correct baseline, the method of double DSC runs was performed under the same conditions. The first DSC curve reflects the case when the ausferrite structure decomposition takes place; the second run is performed on the same sample after the decomposition of ausferrite. The difference, nearly independent of thermophysical properties of the material, shows a non-reversible process of the decomposition of ausferrite during slow heating of ADI sample.

Observations of structure were performed by means of light microscope Neophot 32. Samples of examined alloys were etched with 2% nital to reveal the details of the matrix.

Volume fraction (v_α) of ferromagnetic phase (ferrite) was determined using a simplified magnetic probe method [9] and volume ratio of austenite (v_γ) was calculated according to the formula:

$$v_\gamma = 1 - (v_a + v_g) \quad (3)$$

where v_g is a value of volume fraction of graphite, constant for the examined alloy.

Brinell hardness HB(S) tests were performed using a 2.5 mm diameter steel ball as an indenter with a 1.84 kN force.

Results and discussion

Figure 2a and b shows exemplary differential dilatometric curves of alloy B2, representing the processes that occur during heating of the alloy after previous heat treatments (T_{pi} = 270 and 350 °C, respectively). Generally, several effects could be identified (Fig. 2a) and were marked as I–VII. Similar thermal effects of the phase transformations occurring during non-isothermal decomposition are visible in various proportions on the all dilatometric curves.

Figure 3a and b shows exemplary DSC curves plotted for alloy B2; they show decomposition processes evoked by heating of the alloy after previously performed heat treatments (T_{pi} = 270 and 350 °C, respectively). The compatibility of dilatometric (Fig. 2a, b) and DSC (Fig. 3a, b) curves is evident.

To identify phase transformations revealed during heating, a simple experiment was performed. The samples after two predetermined ADI heat treatments at T_{pi} = 270 °C for 20 min and at T_{pi} = 270 °C for 120 min (processing window) were heated up at a rate of 5 K/min to the temperature T_m of the successively occurring effects (peaks) II, IV, VI, and VII. Then, as soon as the required effects had been achieved, the samples were rapidly removed from the furnace. After cooling in the air, the measurements of hardness HB were carried out and volume fraction v_γ of the carbon-rich austenite was estimated.

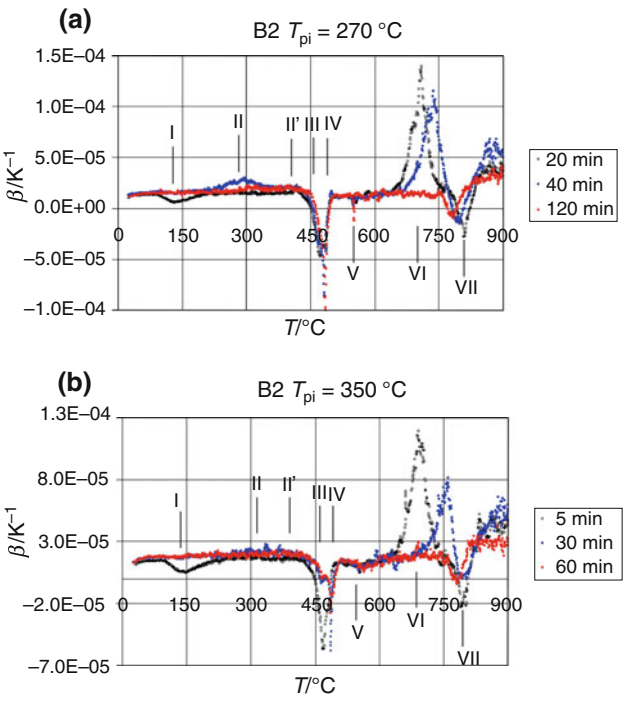

Fig. 2 Differential dilatometric curves of alloy B2; (**a**) T_{pi} = 270 °C, t_{pi} = 20, 40, and 120 min, (**b**) T_{pi} = 350 °C, t_{pi} = 5, 30, and 60 min

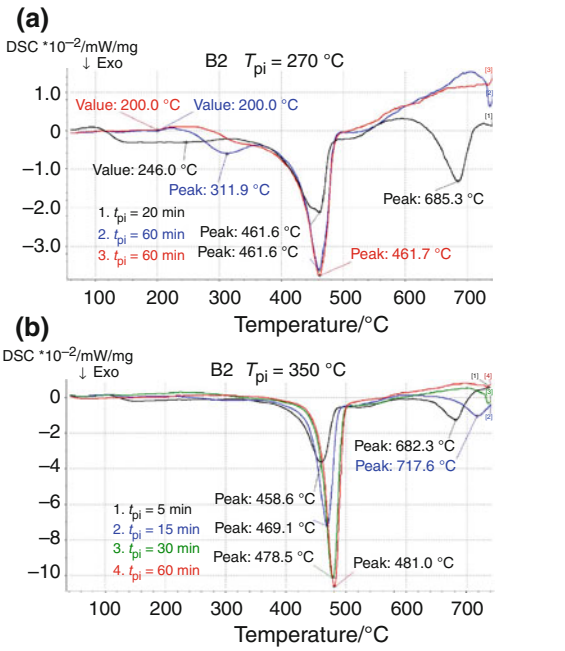

Fig. 3 DSC curves of alloy B2; (**a**) T_{pi} = 270 °C, t_{pi} = 20 min (1), 60 min (2), and 120 min (3), (**b**) T_{pi} = 350 °C, t_{pi} = 5 min (1), 15 min (2), 30 min (3), and 60 min (4)

Figure 4a and b shows a resume of the experiments carried out for the investigated alloy; the filled plotted points correspond with the optimum austempering heat treatments.

The initial structures after austempering heat treatment at 270 °C for 20 min and at 270 °C for 120 min are presented in Fig. 5a and b. The metallographic observations of samples rejected from the furnace after some distinguishable stages of the experiment (peaks III, IV, VI, and VII) are shown in Figs. 6, 7, 8, and 9.

In the case of austenite which has not been sufficiently saturated with carbon, martensite forms during cooling of the sample to room temperature. Effect I characterized by negative volume change on dilatometric curves and low-temperature DSC exothermic peak (Figs. 2, 3) reflects the tempering of martensite present in the matrix of the examined alloy.

Effect II (positive volume changes and exothermal DSC effect) is visible in all the alloys and its position shifts towards higher temperature as the holding time t_{pi} increases, proving an increase of the phase stability. Consequently, overlapping of effects II and III occurs. The increase of the volume change proves that effect II

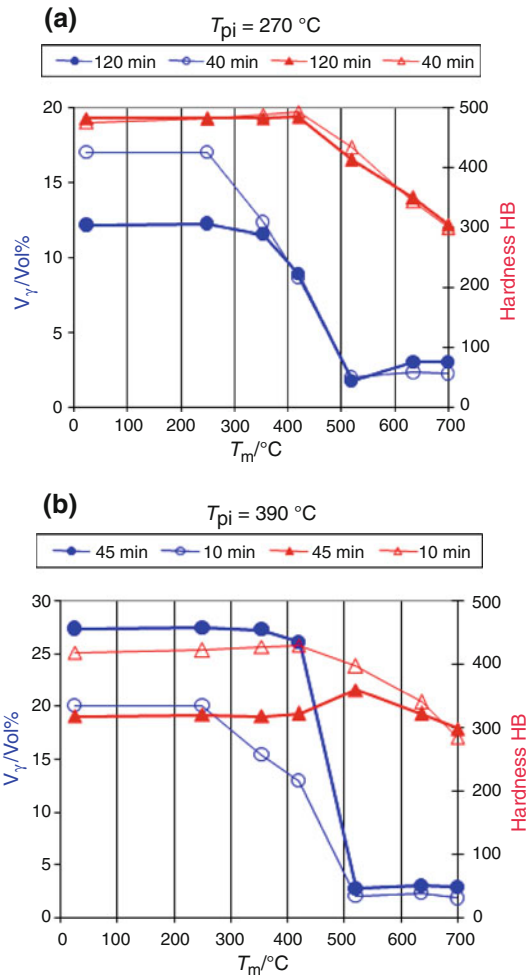

Fig. 4 Dependence of volume fraction v_s and hardness HB on reheating temperature T_m for alloy B2 after previous heat treatment for various holding times at T_{pi} = 270 °C (**a**) and T_{pi} = 390 °C (**b**)

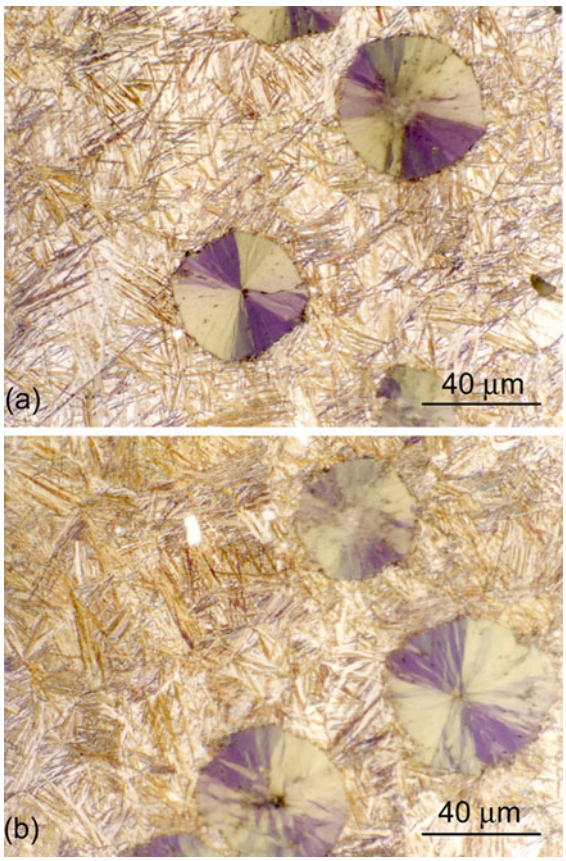

Fig. 5 Metallographic cross-section after etching; austempering heat treatment (**a**) 270 °C/20 min, (**b**) 270 °C/120 min

corresponds to the retained austenite decomposition (the phase with the least specific volume) and microstructure remains unchanging (Fig. 6a, b). The decrease in the amount of retained austenite begins at a relatively low temperature. The overlapping effect II′ is related with an initial stage of carbon precipitation from supersaturated acicular ferrite (Fig. 7a, b).

The double dilatometric effect (III/IV) characterized by contraction ($\Delta V < 0$) and corresponding, strong exothermal DSC peak is generally identified [8, 10–15] as ausferrite decomposition which occurs according to the formula (2). The deconvolution of complex peaks appearing in differential dilatometric curves was accomplished by introducing an extra peak (IV) as the effect of stress relaxation in a very narrow range of temperatures. The enlarged part of Fig. 2b exposing peaks III and IV is shown in Fig. 10. In the case of optimum austempering heat treatment (T_{pi} = 350 °C, t_{pi} = 60 min) the relative total volume change $\Delta V/V$ of double effects is smaller and they are much more isolated than in the alloy after non-optimum heat treatment.

The DSC curves maintain their complex nature over the whole range of the heating temperatures up to a point of the eutectoid transformation, but distinct exothermic effects

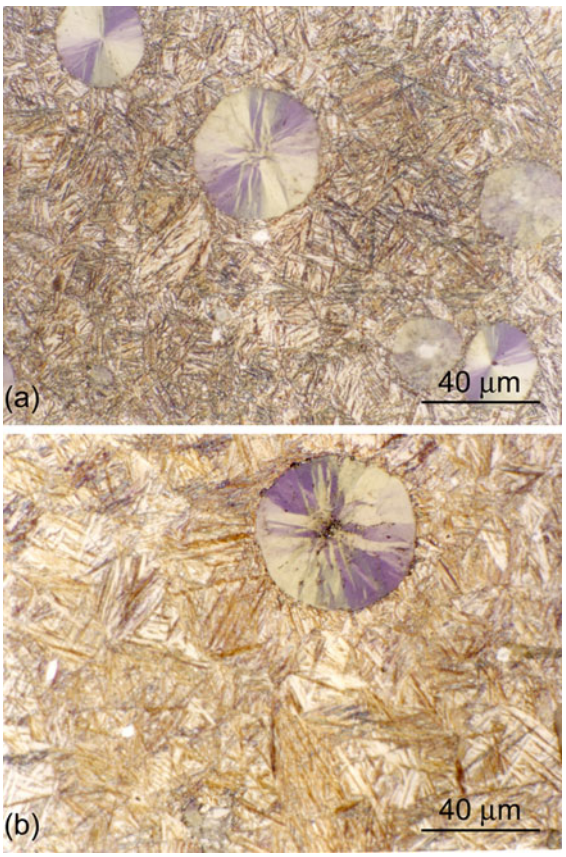

Fig. 6 Metallographic cross-section after etching; $T_m = 420$ °C, ADI heat treatment (**a**) 270 °C/20 min, (**b**) 270 °C/120 min

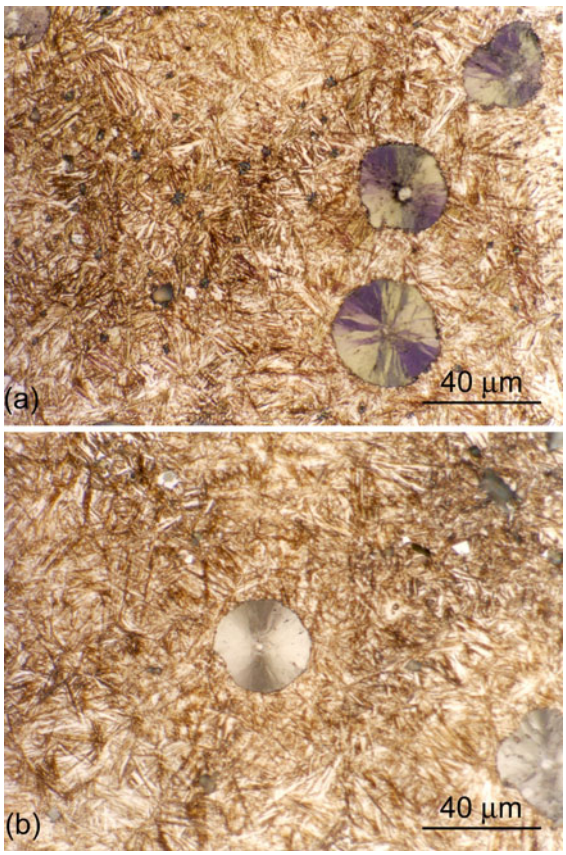

Fig. 7 Metallographic cross-section after etching; $T_m = 530$ °C, ADI heat treatment (**a**) 270 °C/20 min, (**b**) 270 °C/120 min

(400–500 °C) are attributed to the main processes of ausferrite decomposition. The surface areas of the DSC peaks (ΔH) increase and their temperature maxima shift to higher values with the increasing temperature and time of the isothermal transformation (Fig. 3a, b). It proves that the amount of high-carbon austenite and carbon content increase in carbon-rich austenite. Then the peaks become narrower and less complex, thus proving the disappearance of low-carbon austenite. The prevailing nature of exothermal effects signalizes the precipitation processes. The overlapping effects II–IV, which can be found in DSC, and dilatometric curves make the qualitative analysis by means of thermal methods difficult.

The results of the experiments presented in this paper reveal and identify the main, complex effects visible in dilatometric (Fig. 10) and DSC curves (Fig. 3) as peaks III and IV. In the range of 400–500 °C, a complete decomposition of the carbon-rich austenite has occurred (Fig. 8a, b). This statement is entirely prove by decreasing of high-carbon austenite amount visible in Fig. 4a and b. This effect begins at a lower temperature, especially when the temperature of isothermal transformation is low and/or the transformation dwell time is too short to form a stable, high-carbon austenite.

For higher austempering temperature and optimum heat treatment parameters, even a small increase of hardness is observed in the range of 400–500 °C simultaneously with high-carbon austenite decomposition, proving the good stability of acicular ferrite. After exceeding the temperature of 500 °C, a slight decrease of the hardness is observed, reaching finally the near initial value.

The exothermal effect V due to volume decrease can be described in terms of the coagulation of cementite, precipitated from high-carbon austenite. Therefore, this effect is strongly dependent on amount of high-carbon austenite.

The precipitation exothermal (DSC) effect VI characterized by volume increase on dilatometric curve ends there where the eutectoid transformation (effect VII) begins. Effect VI does not depend on the temperature of isothermal transformation and shows a strong tendency to decreasing and shifting towards higher temperatures as the holding time of isothermal transformation increases to approach an optimum value. Figure 9a and b shows that there are much finer graphite precipitates in the alloy tempered after optimum (processing window) austempering than there are in the alloy after non-optimum heat treatment. The effect corresponds to the graphitization of cementite below A_{c1} temperature. Positive volume change arising from

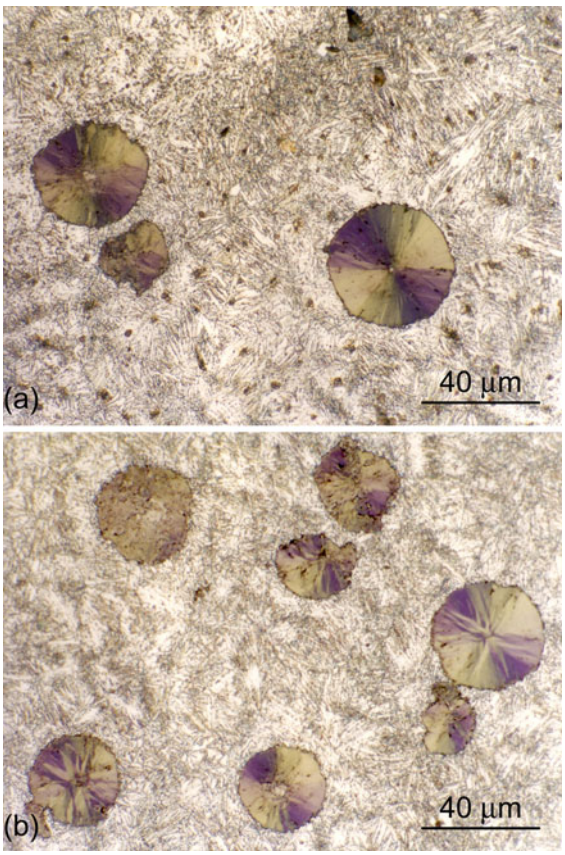

Fig. 8 Metallographic cross-section after etching; $T_m = 680$ °C, ADI heat treatment (**a**) 270 °C/20 min, (**b**) 270 °C/120 min

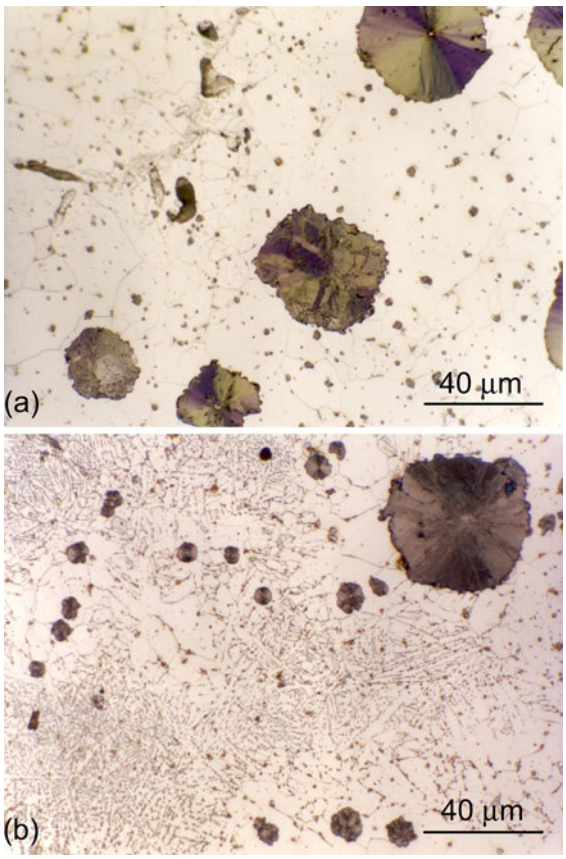

Fig. 9 Metallographic cross-section after etching; $T_m = 790$ °C, ADI heat treatment (**a**) 270 °C/20 min, (**b**) 270 °C/120 min

graphitization is compensated by a negative one resulting from the coagulation of cementite, especially efficiently in the case of optimum austempering heat treatment.

The metallographic examinations (peaks III, IV, VI, and VII) presented in Figs. 5, 6, 7, 8, and 9 show that the acicular structure of ferrite is preserved up to a relatively high temperature and just before the temperature of the eutectoid transformation of ferrite (effect VI) has appeared.

Table 2 contains a summary of qualitative analysis and identification of phase transformations generated during controlled heating of the investigated alloy with the mixed ausferritic and martensitic structures. The scheme of decomposition of ausferrite structure, inclusive of the settlements with regard to martensite tempering [1, 4–7] was proposed.

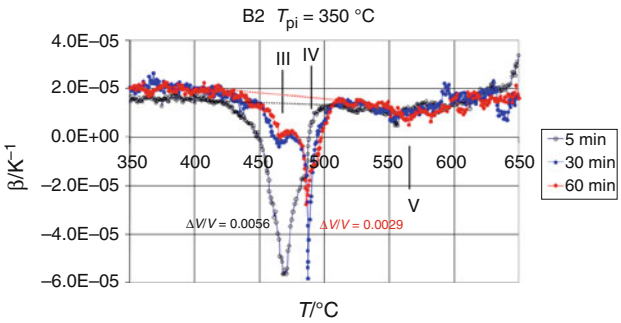

Fig. 10 Part of differential dilatometric curve of alloy B2; $T_{pi} = 350$ °C, $t_{pi} = 5$, 30, and 60 min

Conclusions

The carried out investigations and analysis of the results of experiments on copper-nickel austempered ductile iron allow the following conclusions to be formulated:

- The method of analysis consisting in investigation of the inverse phase transformations by means of controlled heating of the structurally well-defined material with simultaneous recording of thermophysical properties by means of differential scanning calorimetry (DSC) and differential dilatometry was successfully applied.
- The paths of decomposition of austempered ductile iron while heated up to ca 800 °C were recognized and discussed, and the scheme of ausferrite decomposition was established and summarized in Table 2.
- For optimum (processing window) ADI heat treatment, the stability of ausferrite during non-isothermal tempering up to 400 °C was proved.

Table 2 The identification of phase transformations proceeding during thermal decomposition of copper–nickel ADI, based on DSC and dilatometric investigations

Effect	T (°C)	Initial structure		Transformation	Final structure		DIL	DSC
I	80-200	As-quench martensite α'	supersaturated tetragonal ferrite (α_{tetr})	$\alpha_{tetr} \rightarrow \alpha_{sac} + \varepsilon(\eta)$ stress relaxation	Supersaturated acicular ferrite (α_{sac})	Tempered martensite α'_{temp}	$\Delta V < 0$	EXO
					Coherent carbides $\varepsilon (Fe_{2,4}C)$ or η (Fe_2C)			
			retained austenite (γ_r)		γ_r			
		Ausferrite	supersaturated acicular ferrite (α_{sac})		α_{sac}	Ausferrite		
			carbon-rich austenite (γ_s)		γ_s			
II	200-300	α'_{temp}	α_{sac}		α_{sac}	α'_{temp}	$\Delta V > 0$	EXO
			ε		ε			
			γ_r	$\gamma_r \rightarrow \alpha_{sac} + \varepsilon(\eta)$	α_{sac}			
					Coherent carbides $\varepsilon(\eta)$			
		Ausferrite	α_{sac}		α_{sac}	Ausferrite		
			γ_s		γ_s			
II'	300-400	α'_{temp}	α_{sac}	$\alpha_{sac} \rightarrow \alpha_{ac} + Fe_3C$	Accicular ferrite (α_{ac})	Troostite	$\Delta V < 0$	EXO
					Cementite Fe_3C			
			ε	$\varepsilon \rightarrow Fe_3C$	Fe_3C (coherency lost)			
		Ausferrite	α_{sac}	$\alpha_{sac} \rightarrow \alpha_{ac} + Fe_3C$	α_{ac}	Ausferrite		
					Fe_3C			
			γ_s		γ_s			
III IV	400-520	Troostite	α_{ac}		α_{ac}	Tempered sorbite	$\Delta V < 0$	EXO
			Fe_3C	Coagulation	Fe_3C			
		Ausferrite	α_{sac} or/and α_{ac}	$\alpha_{sac} \rightarrow \alpha_{ac} + Fe_3C$ stress relaxation	α_{ac}	Troostite		
					Fe_3C			
			γ_s	$\gamma_s \rightarrow \alpha_{ac} + Fe_3C$	α_{ac}			
					Fe_3C			
V	> 520	Sorbite	α_{ac}		α_{ac}	Sorbite	$\Delta V < 0$	EXO
			Fe_3C	Coagulation	Fe_3C			
		Troostite	α_{ac}		α_{ac}			
			Fe_3C	Coagulation	Fe_3C			
VI	> 650	Sorbite	α_{ac}	recrystallization Curie Point	Ferrite (α)	Divorced pearlite, ferrite, C_{gr}	$\Delta V > 0$	EXO
			Fe_3C	$Fe_3C \rightarrow C_{gr} + \alpha$ (graphitization)	Fe_3C, α and graphite precipitates C_{gr}			
VII	~ 770	Pearlite Ferrite C_{gr}	α, Fe_3C, C_{gr}	Eutectoid transformation	γ	Austenite	$\Delta V < 0$	ENDO

- For optimum ADI heat treatment, a complete decomposition of the carbon-rich austenite has occurred in the range of 400–500 °C, giving rise to the small increase of hardness resulting from Fe_3C precipitation.
- The results of the designed experiment and metallographic examinations proved that the acicular ferrite is preserved up to a relatively high temperature of non-isothermal ADI tempering.
- The shape of ausferrite decomposition effects on dilatometric curves (peaks III, IV, and V) allow to distinguish between the grades of ADI characterized by definite amounts of high-carbon austenite and acicular ferrite, depending on temperature of isothermal transformation.
- Very distinctive, positive dilatometric effect VI corresponding to exothermal DSC peak shows a tendency to decreasing and shifting towards higher temperatures as a time of the isothermal transformation increases to approach an optimum value and can be identified as a resultant of cementite coagulation and graphitization processes.
- The absence of effect VI (coagulation and graphitization) seems to be an adequate measure of proper choice of optimum austempering heat treatment parameters.
- The elaborated decomposition scheme allows rational estimation and selection of the ADI heat treatment type (standard, two-step, non-isothermal) and its optimization by application of the non-isothermal thermal analysis methods—dilatometry and DSC.

Acknowledgements This work was financially supported by Polish Committee of Scientific Research (KBN); Grant No. 4 TO8B 031 entitled: "Investigation of thermal stability and optimization of heat treatment parameters of Cu–Ni ADI by means of thermal analysis method".

References

1. Morra PV, Böttger AJ, Mittemeijer EJ. Decomposition of iron-based martensite A kinetic analysis by means of differential scanning calorimetry and dilatometry. J Therm Anal Calorim. 2001;64:905–14.
2. Birol Y. DSC analysis of the precipitation reaction in AA6005 alloy. J Therm Anal Calorim. 2008;93(3):977–81.
3. Carvalho TM, Silva RAG, Adorno AT, Magdalena AG. Ag-rich phase precipitation in the Cu–9 mass% Al alloy with Ag additions. J Therm Anal Calorim. 2009;97(1):53–6.
4. Cast steel: the tempering of martensite: Part One. Web source: http://steel.keytometals.com/Articles/Art127.htm.
5. Cast steel: the tempering of martensite: Part Two. Web source: http://steel.keytometals.com/Articles/Art128.htm.
6. Przemiany odpuszczania. Web source: http://www.immt.pwr.wroc.pl/~ziolek/Pliki/TW3%20OC3%2016.10.2009.pdf.
7. Goji M, Su M, Raji M. Thermal analysis of low alloy Cr–Mo steel. J Therm Anal Calorim. 2004;75:947–56.
8. Gazda A. Determination of thermal effects accompanying the austempering of copper–nickel ductile iron. Thermochim Acta. 2010;499(1–2):144–48.
9. Maryniak WA, Uehara T, Noras MA. Surface resistivity and surface resistance measurements using a concentric ring probe technique. Trek Application Note; 2003, No. 1005:1–4. Web source: http://www.trekinc.com/pdf/1005_Resistivity_Resistance.pdf.
10. Baricco M, Franzosi G, Nada R, Battezzati L. Thermal effects due to tempering of austenite and martensite in austempered ductile irons. Mater Sci Technol. 1999;15:643–46.
11. Nadkarni S, Gokhale S, Boyd JD. Elevated temperature microstructural stability of austempered ductile irons. AFS Trans. 1996;104:985–94.
12. Massone JM, Boeri RE, Sikora JA. Decomposition of high-carbon austenite in ADI. Trans AFS. 1996;20–23:133–7.
13. Bayati H, Elliott R. Aging process of alloyed ADI. Second international conference on processing materials for properties, San Francisco, CA, USA; 2000, pp. 77–82.
14. Gazda A. Kinetics of the bainitic transformation proceeding in austempered ductile iron. Acta Metall Slov. 2001;7:74–9.
15. Perez MJ, Cisneros MM, Valdes E, Mancha H, Calderon HA, Campos RE. Experimental study of the thermal stability of austempered ductile irons. J Mater Eng Perform. 2002;11(5):519–26.